Experimental and numerical investigations of low energy/velocity impact damage generated in 3D woven composite with polymer matrix

A. Elias, Frédéric Laurin, Myriam Kaminski, Laurent Gornet

Experimental and numerical investigations of low energy/velocity impact damage generated in 3D woven composite with polymer matrix

A. Elias [a], F. Laurin [a,*], M. Kaminski [a], L. Gornet [b]

[a] ONERA, 29 avenue de la Division Leclerc, F-92322 Châtillon, France
[b] GeM UMR CNRS 6183, Ecole Centrale de Nantes, 1 rue de la Noë, F-44321 Nantes, France

3D woven composite materials have been recently used to design some engine structures in order to improve their impact resistance. The aim of this work is to study experimentally and numerically low-velocity/energy impact damage in such recent composites. Impact tests at different energy levels have been performed and analysed using microscopic observations and X-ray tomography in order to understand damage mechanisms occurring in this material. Finite element simulations have been performed using the continuum damage model, ODM-PMC, developed at Onera for 3D woven composites under static loadings. Through comparisons with the available experimental data, it has been demonstrated that the damage mechanisms are described correctly by the present model. Moreover, the residual depth after impact is also accurately predicted, allowing to generate, numerically, relations between impact energy, damaged area and residual depth, currently determined experimentally in aeronautical industries.

1. Introduction

Some critical components of aircraft structures, such as centre wing box, wings or fuselage, are now manufactured with laminated composite materials, due to their high specific mechanical properties. However, these materials are particularly sensitive to low-velocity/energy impact events such as dropped tools. These impacts on laminated composite structures generate large damaged areas inside the laminate while leaving a barely visible indent on its impacted surface. Moreover, such a damage induces a strong decrease in the residual strengths after impact [1,2], and has obliged the designers in aeronautics to use large safety margins, thus decreasing the competitiveness of carbon fibre reinforced polymer composites as compared to metallic materials. Therefore, the impact resistance of laminated composites manufactured with unidirectional plies has been widely studied for many years [1–3] from both an experimental and a numerical point of view. Experimental studies have shown that a low-velocity/energy impact induces mainly three types of damage [4–6]: large delamination cracks between plies with different orientations, matrix cracking in the different plies and also, for high enough impact energy levels, fibre failures. Due to delamination, a marked loss of residual strengths, especially under compressive loading [7], is observed for such a material. For classical Carbon/Epoxy materials, the failure of pre-impacted specimens subjected to compression is usually due to local buckling [8–10] of the plies because the delamination cracks generated during impact divide the plate into multiple sub-laminates. This local buckling can induce some propagation of delamination to the lateral edges [7] and also fibre failures in compression of some plies (due to fibre kinking). Thanks to these experimental studies, the failure mechanisms and their couplings are currently well understood for flat laminates. Therefore, the description of the large delamination cracks due to impact is clearly a key point in the modelling to predict the residual strength. To describe these discrete large cracks within the laminate, cohesive zone elements [8,11] or interaction cohesive approaches [12,13] are usually used to model delamination (both onset and propagation) in finite element codes. Only few authors [8,14,11] have succeeded in describing accurately the delamination patterns after impact because of numerical difficulties in impact simulation although explicit solvers are usually used. Moreover, very few and recent studies [14,15] have succeeded in performing impact test simulations and then compression after impact.

Due to the poor impact resistance of laminated composite materials, 3D woven composites have been recently developed to be used in structures exposed to impact. Indeed, the main advantage of these materials consists in preventing large delamination cracks thanks to the presence of yarns linking the layers together. The use of these materials for industrial applications being recent,

* Corresponding author.
E-mail address: frederic.laurin@onera.fr (F. Laurin).

only few experimental studies [4,16,17] have been dedicated to the influence of such an architecture on impact and post-impact behaviour. The observed damage mechanisms in 3D woven composites are very different from those encountered in classical laminates due to the specific architecture of such materials. Due to the complexity of the encountered damage mechanisms, only very few impact modelling studies [18] can be found in the literature and are dedicated to very specific architectures.

This work is thus dedicated to the experimental and numerical study of the damage induced by low-velocity/energy impacts, representative of dropped tools, in a new generation of 3D woven composite materials. Moreover, the present article aims to demonstrate that the Onera Damage Model for Polymer Matrix Composites (ODM-PMC), based on the continuum damage approach, is relevant for such materials and allows predicting the different quantities of interest such as damage patterns, maximum peak loads and residual dents.

Firstly, an experimental study has been performed in order to improve the understanding of the different damage mechanisms induced by impact loading through the analysis of impact damage at different energy levels. This experimental investigation is reported in Section 2. The studied 3D woven material developed by Safran Group is briefly described in Section 2.1. The experimental setup and the different measurement techniques to study the damage generated after impact are presented in Section 2.2. In Section 3, the ODM-PMC model, initially developed for 3D woven composite structures under static loadings, is presented. Then, in Section 4.1, this approach has been implemented into a finite element code to predict damage after impact at different energy levels. The details of the finite element simulations (mesh, boundary conditions ...) are given in Section 4.2. The identification process of the different parameters of this approach is also presented in Section 4.3. Finally, in Section 4.4, the comparisons between the different experimental data and the predictions of the simulations performed with ODM-PMC are presented and discussed.

2. Impact test results

2.1. 3D woven composite material

The material under investigation is a moderately unbalanced 3D woven composite material provided by Safran Group, already studied in [19], and consisting of carbon fibre yarns (48 K) embedded in an epoxy matrix. Based on the generic architecture reported in Fig. 1, the studied 3D woven composite material has been designed by Safran group in order to prevent large delamination after impact and thus to obtain good impact resistance (the exact architecture of this material is, however, confidential). The thickness of the tested material is about 11.5 mm, which is rather thick as compared to previously studied laminates or 3D woven composites. It is worth mentioning that the Representative Elementary Volume of such a material is rather large (a few centimetres) as compared to other composite materials and thus imposes to use large plates and a large diameter impactor.

2.2. Experimental device

Drop-weight impact tests on 3D woven polymer matrix composites have been performed in a Dynatup 8250 (GRC Instruments) apparatus, as illustrated in Fig. 2. During the tests, the force history has been measured with a force cell located in the impactor and the displacement history of the point opposite to impact has been measured using a laser sensor.

Due to the thickness of the specimens, the experimental device recommended in the ASTM D7136/D7136M standard [20] cannot be considered in the present study. Therefore, two different alternative experimental devices have been used in this study. It is essential to note that the boundary conditions of these two test configurations can be easily introduced into a finite element simulation, in order to analyse experimentally and numerically the available test results. The first configuration, reported in Fig. 2a, consists in holding the plate by two square jaws with a circular free zone, which diameter is equal to 70 mm. This experimental setup has been chosen in order to understand the damage and failure mechanisms encountered in 3D woven composite materials and also to be compared with finite element simulations to validate the proposed modelling. For this configuration, the dimensions of the tested plates are 100 mm $\times$ 100 mm $\times$ 11.5 mm. The steel-made impactor is hemispheric (40 mm in diameter) and its mass is set to 14.8 kg. Due to the architecture of the 3D woven composite material, the diameter of the impactor is quite large; it has been chosen in order to avoid impacting only one fibre yarn or only the matrix between yarns. Four different energy levels (60 J, 100 J, 150 J and 210 J) have been considered by changing the velocity set through adjustment of the height of the drop weight. Each test has been repeated two or three times to estimate the scattering and has been performed at room temperature. This configuration of tests is referenced in the following as configuration 1.

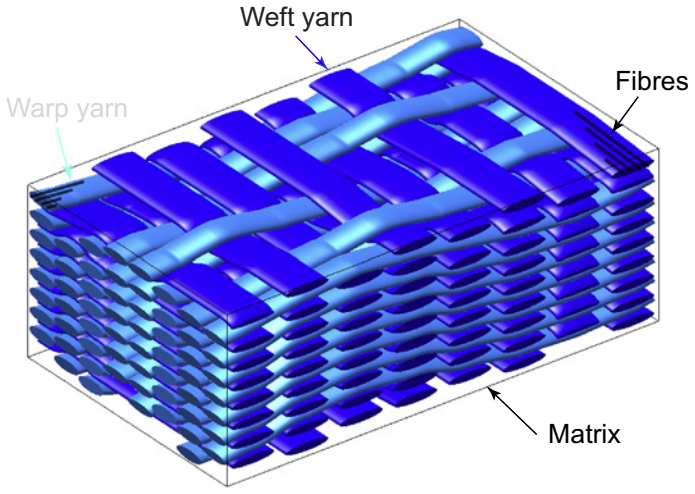

Fig. 1. Generic architecture of an unbalanced 3D woven composite material.

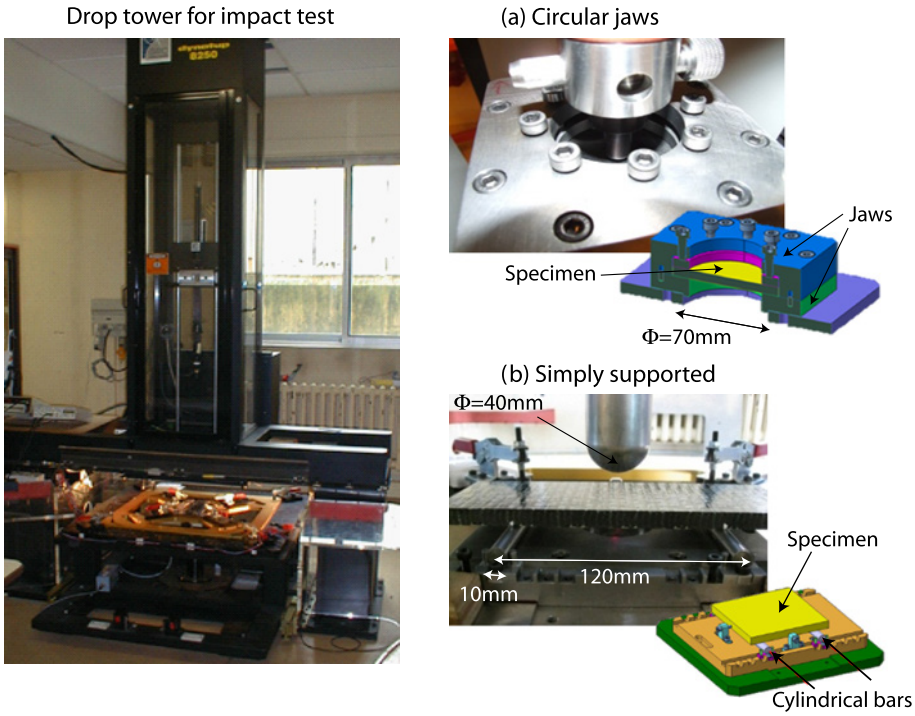

Fig. 2. Drop-weight impact testing setup and specific devices developed at Onera: (a) jaws with a circular free zone and (b) a simply supported device.

Moreover, in order to confirm the damage scenario established through the analysis of the impact tests using the test configuration 1, a second experimental device has been used in this study, as reported in Fig. 2b. The specimen is simply supported by two cylindrical bars (10 mm in diameter). The distance between the two bars has been fixed at 120 mm after preliminary finite element simulations in order to avoid too large a displacement for the three considered energy levels (40 J, 70 J and 80 J), also obtained by changing the velocity set through adjustment of the height of the drop weight. For this configuration, the dimensions of the tested plates are 260 mm × 70 mm × 11.5 mm. These tests have been performed to validate the proposed modelling. Moreover, due to this geometry, these impacted specimens can be then subjected to tensile or compressive loading in order to determine the residual strengths. This configuration of tests is referenced in the following as configuration 2.

2.3. Analysis of impact induced damage

In order to improve the understanding of the different damage mechanisms generated during a low velocity/energy impact, different measurement techniques have been used.

Firstly, a classical ultrasonic analysis (with ultrasonic pulse-waves with centre frequencies at 1 MHz) of the impacted specimens has been performed just after the tests to determine the damaged area. For low energy levels (equal or inferior to 150 J for test configuration 1 and 70 J for test configuration 2), the shape of the damaged area is slightly elliptical, as reported in Fig. 3, which is consistent with the unbalanced woven architecture. Contrary to laminates, back wall echo is always recorded, thereby suggesting that no large delamination is detected; the decrease in amplitude measured by C-Scan is thus probably due to diffuse damage within the material. The damaged area increases linearly as a function of the energy impact. For higher energy levels, the shape of the damaged area is clearly influenced by the boundary conditions (circular for configuration 1, due to interactions with the jaws, and rectangular, because of interactions with free edges, for configuration 2).

Then, some plates have been cut through the damaged area in different directions (0°, 45°, 90°) and polished in order to observe carefully the different damage mechanisms occurring during impact tests. Microscopic observations have been performed on the polished cross sections. These observations, reported in Fig. 4, show that damage mechanisms are mainly inter-yarn debondings and in-plane matrix cracking. The numerous observed diffuse damage mechanisms are clearly oriented by the architecture of the material. Inter-yarn debondings and typical matrix shear cracks are observed through the thickness and follow the out-of plane shear stress gradients. Straight matrix cracks are observed close to the back face of the plate which is subjected to a local in-plane tensile loading due to the global bending of the plate. Finally, no (or very few) damage is observed directly under the contact zone between the plate and the impactor, this zone being subjected to a multiaxial state of stress which is nearly a hydrostatic compression. Indeed, the hydrostatic pressure may reinforce the apparent strength of the material and prevents the creation of cracks as already observed for laminated composites [21]. It can be noted that similar damage patterns constituted of inter-yarn debondings and matrix cracking (due to tensile or out-of-plane shear stresses) are observed in specimens impacted with test configuration 2.

These observations have been extended through the analysis of other specimens through X-ray tomography to estimate the three dimensional distribution of damage within the material, as already performed in previous experimental studies on unidirectional plies [22,10] and other 3D woven materials [23]. The X-ray tomography has been performed by Safran Composite. The whole specimen has been scanned with a voxel resolution of 38 μm. The previous conclusions, established through microscopic scale observations, are confirmed through the analysis of X-ray tomographs, increasing thus the confidence in these two measurement techniques. Moreover, as reported in Fig. 5 for a specimen impacted at 60 J, only dif-

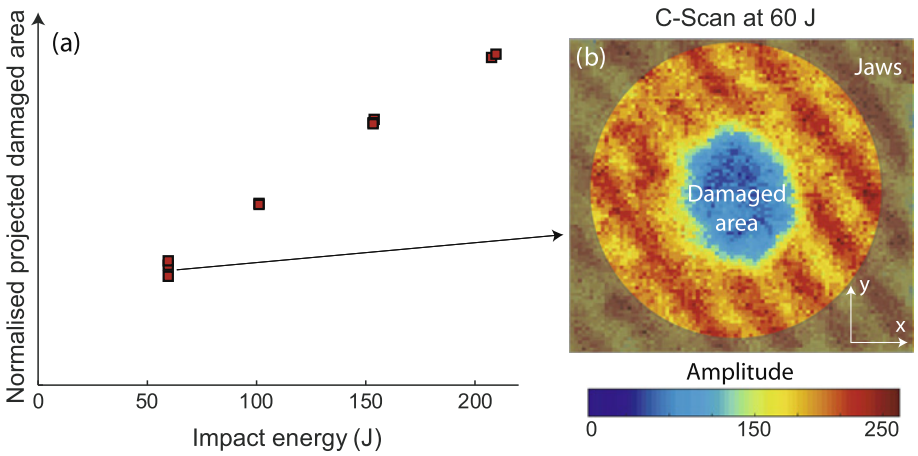

Fig. 3. (a) Evolution of the damaged area measured by C-Scan as a function of the impact energy levels for configuration 1. (b) C-Scan of a 60 J impacted 3D woven specimen where the x-direction is aligned with the warp direction.

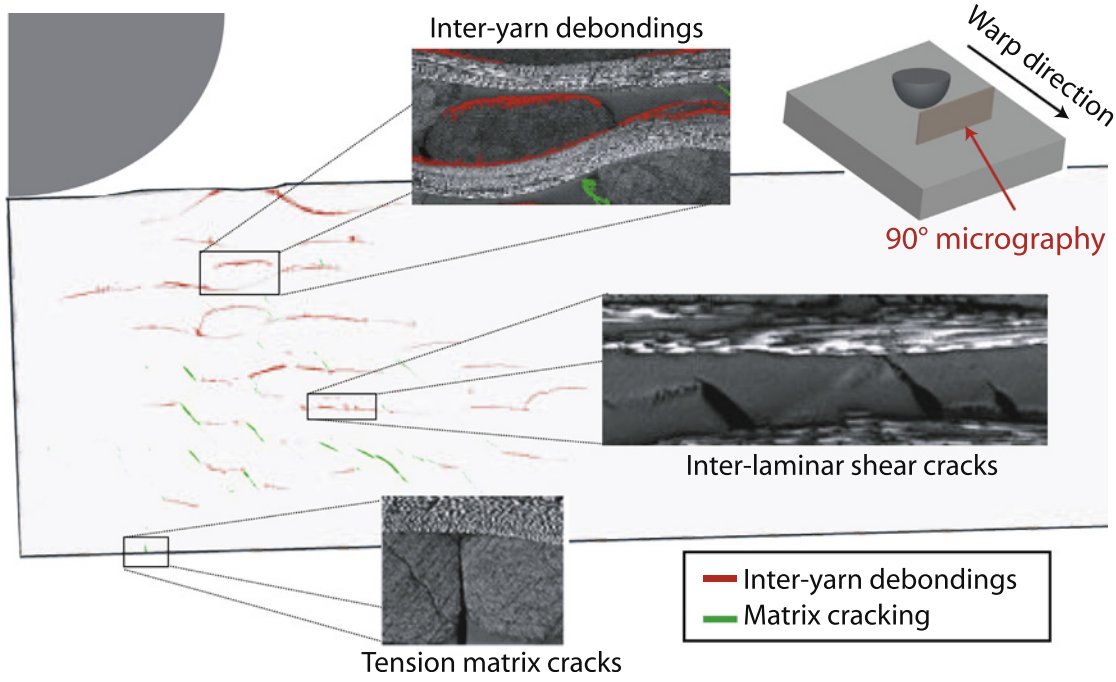

Fig. 4. Microscopic observations of the different damage mechanisms within a 100 J impacted 3D woven plate for configuration 1.

fuse damage (mainly inter-yarn debondings and few matrix cracking) is observed. Contrary to the laminates manufactured with unidirectional plies or 2D woven plies, no large delamination is observed after impact because of the specific architecture. Therefore, the use of continuum damage models for such a material is relevant, as detailed in Section 3.

2.4. Residual depths

The residual indentation depth is the only visible marker which indicates that the structure has been impacted and probably damaged and is thus essential for the management of maintenance of composite parts. Therefore, in this study, the residual indentation depth has been measured through digital stereo-correlation using two CCD cameras (12 bits with a resolution: 2000 × 2000 pixel^2) and the commercial Vic3D system©. The residual indentation presents an elliptical shape, consistent with the unbalanced architecture, and its depth evolves linearly as a function of the impact energy levels, as reported in Fig. 6a. Moreover, to improve the understanding of this residual indentation depth, these measurements have been performed for some specimens at different times after impact to estimate the evolution of the indentation depth. For the highest incident energy tests (210 J), relaxation is observed since indentation depth decreases around 8% after the first 48 h after impact (see Fig. 6b), suggesting that only a small part of the residual indentation can be attributed to viscosity of the matrix. Some authors have attributed the indentation depth to debris in matrix cracking [24,25] within laminates. For 3D woven composites, the residual indentation is probably related to the complex morphology of the observed cracks oriented by the microstructure as reported in Fig. 4, and potentially to debris (whereas none has been explicitly detected in microscopic observations).

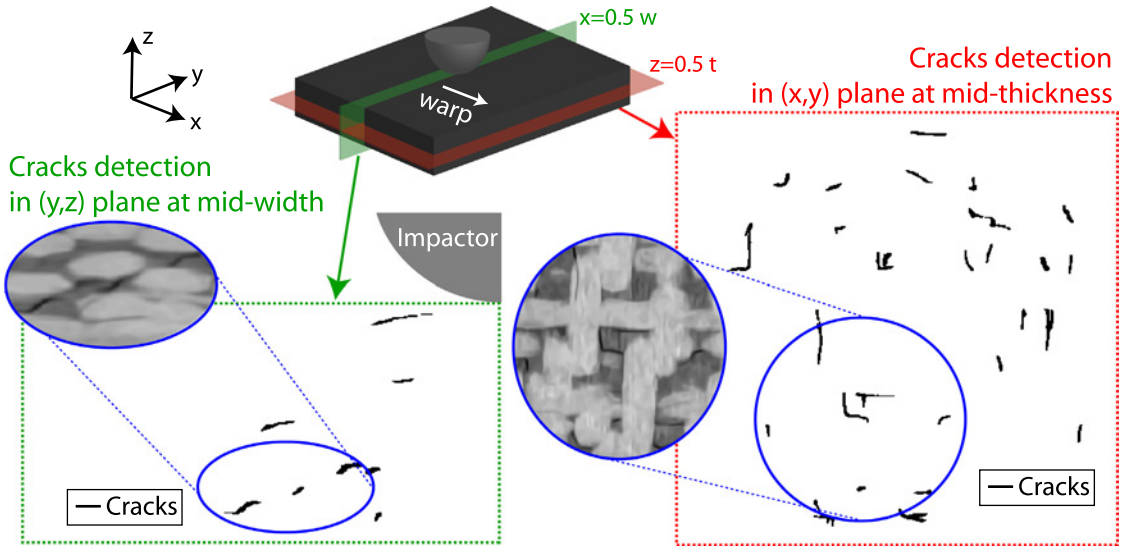

Fig. 5. X-ray tomography of a 60 J impacted 3D woven plate for configuration 1.

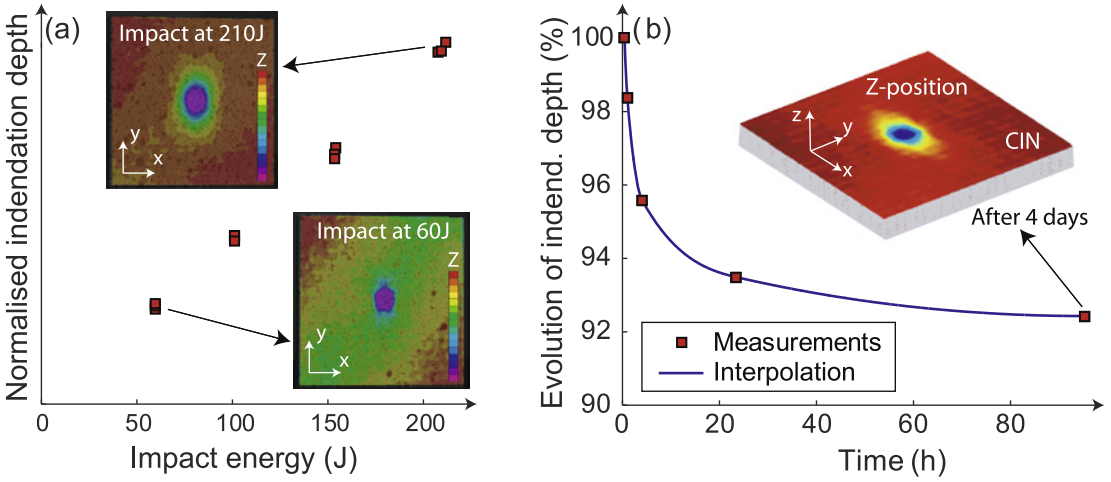

Fig. 6. Evolution of the residual indentation depth (a) as a function of the impact energy for configuration 1 and (b) as a function of time after an impact at 210 J.

3. Presentation of the ODM-PMC model

3.1. General presentation of the model

As mentioned in Section 2.3, only diffuse damage (inter-yarn debondings and in-plane matrix cracking) is observed contrary to damage studied in laminates which mainly consists in large delamination cracks. Therefore, the modelling approach suitable for such a material should be very different from those used for laminates, which are mainly based on Cohesive Zone Modelling [8,14,11].

The Onera Damage Model for Composites with Polymer Matrix (ODM-PMC) is thus based on continuum damage approaches [26] and is defined at the macroscopic scale in order to be used in design offices for the strength predictions of composite structures representative of industrial components. For new generations of 3D woven composites, multiple sources of non-linearity have been determined experimentally [27–29] through the analysis of static and fatigue tests performed in previous studies.

It has been demonstrated that the ODM-PMC model is able to predict the non-linear behaviour, damage and failure of 3D woven composites subjected to quasi-static and fatigue loadings [30,31,29]. In the present article, the predictive capabilities of this model for impact cases are evaluated. Only the main ideas of this model are presented, special attention being paid to the non-linearities which play a major role for impact loadings. The present approach is thermodynamically consistent and the macroscopic behaviour, expressed in Eq. (1), derives directly from the Helmholtz free energy.

$$\underline{\sigma} = \underline{\underline{C}}^{eff} : (\underline{\varepsilon} - \underline{\varepsilon}^{ve} - \underline{\varepsilon}^{0}) - \underline{\underline{C}}^{0} : (\underline{\varepsilon}^{s} - \underline{\varepsilon}^{r} - \underline{\varepsilon}^{0}) \quad (1)$$

where $\underline{\sigma}$ is the stress tensor, $\underline{\varepsilon}$ the total strain tensor, and $\underline{\varepsilon}^{ve}$ the viscoelastic strain tensor. Taking into account the viscosity of the polymer matrix is essential to describe accurately the macroscopic behaviour of specimens subjected to quasi-static off-axis tension with different strain rates or creep loading. On the contrary, for impact test cases, the viscosity plays only a minor role in the evolution of the different damage mechanisms because sufficiently high loading rates are involved and, as demonstrated previously, its influence on the permanent indentation is also limited. The viscoelastic approach used in the present study is thus not detailed in this paper, but more information can be found in [32,33].

In Eq. (1), $\underline{\underline{C}}^{0}$ corresponds to the initial elastic stiffness tensor and $\underline{\underline{C}}^{eff}$ is the effective elastic stiffness tensor taking into account

the effects of the different damage and failure mechanisms, as expressed in Eq. (2).

$$\underline{\underline{C}}^{eff} = \underline{\underline{S}}^0 + \sum_{i=1}^{2} d_i \underline{\underline{H_i^m}} + D_3 \underline{\underline{H_3}} + \sum_{j=1}^{2} \left[D_j^t \underline{\underline{H_j^{D_t}}} + D_j^c \underline{\underline{H_j^{D_c}}} \right] \Bigg)^{-1} \quad (2)$$

For such a material, the high contrast between the mechanical properties of the constituents (matrix and fibre yarns) leads to crack orientations induced by the microstructure. Therefore, each damage or failure mechanism is described in the model by a scalar variable. In the present approach, these different damage variables are classified as a function of their effects on the macroscopic behaviour.

Mesoscopic damage variables (d_1 in the warp direction, d_2 in the weft direction) are related to in-plane matrix cracking and induce a notable non-linear effect on the macroscopic behaviour through the term ($\sum_{i=1}^{2} d_i \underline{\underline{H_i^m}}$) in Eq. (2).

The out-of-plane macroscopic damage (D_3) which corresponds to the inter-yarn debondings, appearing under impact loading, plays a major role in the macroscopic behaviour during an impact test and its effects are taken into account through the term ($D_3 \underline{\underline{H_3}}$) in Eq. (2).

For unnotched specimens, the rupture in the material axis is due to the failure of fibre yarns. The macroscopic variables D_1^t and D_2^t describe the effects of yarn failures in tension, respectively, in the warp and weft directions, D_1^c and D_2^c the effects of yarn failures in compression in the warp and weft directions. These yarn failures induce a violent and softening macroscopic behaviour through the term ($\sum_{j=1}^{2} D_j^t \underline{\underline{H_j^{D_t}}} + D_j^c \underline{\underline{H_j^{D_c}}}$) in Eq. (2).

Finally, the ($\underline{\varepsilon}^0, \underline{\varepsilon}^s$) specific strain tensors, which take into account the unilateral aspect of damage in the present model, are detailed in Section 3.3 and the residual strain ($\underline{\varepsilon}^r$) is defined in Section 3.4.

3.2. In-plane matrix cracking and inter-yarn debondings

The driving forces associated with the two in-plane mesoscopic damage variables (d_1, d_2) and to the out-of-plane macroscopic damage variable (D_3) are expressed in Eq. (3).

$$\begin{cases} y_1 = \frac{1}{2}\left(C_{11}^0 \varepsilon_{11}^{m_1^+} + a_{16} C_{66}^0 \gamma_{12}^{m_1^+} + a_{15} C_{55}^0 \gamma_{13}^{m_1^+} \right) \\ y_2 = \frac{1}{2}\left(C_{22}^0 \varepsilon_{22}^{m_2^+} + a_{26} C_{66}^0 \gamma_{12}^{m_2^+} + a_{24} C_{44}^0 \gamma_{23}^{m_2^+} \right) \text{ with } \quad \underline{\varepsilon}^m = \underline{\underline{S}}^{eff} : \underline{\sigma} + \underline{\varepsilon}^{ve} \\ y_3 = \frac{1}{2}\left(C_{33}^0 \varepsilon_{33}^{m_3^+} + a_{34} C_{44}^0 \gamma_{23}^{m_3^+} + a_{35} C_{55}^0 \gamma_{13}^{m_3^+} \right) \end{cases} \quad (3)$$

where driving forces depend on (i) the different components of the initial elastic stiffness tensor, (ii) on the material coefficients ($a_{15}, a_{16}, a_{24}, a_{26}, a_{34}, a_{35}$) and (iii) on the mechanical strain tensor $\underline{\varepsilon}^m$. The use of this mechanical strain in the driving forces, instead of the total strain, allows avoiding unstable evolution of damage during fatigue loadings [31], and also allows simplifying the identification procedure by decoupling the causes of the different damage mechanisms (due to the elastic $\underline{\varepsilon}^e$ and viscoelastic $\underline{\varepsilon}^{ve}$ strains) from their consequences, such as the stored ($\underline{\varepsilon}^s$) and residual ($\underline{\varepsilon}^r$) strains. Moreover, the positive strain tensor used in driving forces corresponds to the positive part, as proposed by [34], of the mechanical strain tensor where all the components are zeros except those inducing damage. The use of the positive strain tensor is an elegant way (i) to capture the reinforcement of the apparent onset of damage for combined compressive and shear loadings [35,36], (ii) to describe the reinforcement of the apparent onset of damage due to hydrostatic pressure [21], without introducing additional coefficients.

Finally, the evolution laws of these damage variables are expressed in Eq. (4), where the parameter y_i^0 corresponds to the onset of damage, d_i^c to the saturation of damage, and (y_i^c, p_i) are parameters which are related to the damage evolution laws. It can be noted that damage can only grow in order to ensure the second principle of thermodynamics. The $< >_+$ corresponds to the classical Macauley brackets.

$$d_i = d_i^c \left(1 - exp\left(- \left(\frac{< \sqrt{y_i} - \sqrt{y_i^0} >_+}{\sqrt{y_i^c}} \right) \right)^{p_i} \right) \quad \text{with} \quad \dot{d}_i \geqslant 0 \quad \text{for} \quad i = \{1,2,3\} \quad (4)$$

3.3. Unilateral aspect of damage

The present section is dedicated to studying the effects of the different damage mechanisms and especially to the necessity of taking into account the unilateral aspect of damage, as it has been demonstrated experimentally in many previous works [31,37,29]. Indeed, by applying a low compressive loading after having generated matrix damage during the tensile loading, a progressive recovery of the initial elastic Young's modulus is observed because of the progressive closure of the cracks due to crack orientation scattering in the damaged material. It is worth mentioning that the introduction of this progressive crack closure allows improving drastically the convergence of finite element simulations for impact problems, since continuity in the material response is ensured, especially in the areas close to the impactor. To describe the progressive deactivation of damage for a tension/compression test in the weft direction in the present approach, the effect tensor $\underline{\underline{H_2^m}}$ associated with the damage variable d_2 is defined as a function of a progressive deactivation index (η_2) describing the effects of a crack on the effective elastic stiffness, as reported in Eq. (5). The progressive deactivation index (η_2) evolves continuously from 0 (closed cracks) to 1 (opened cracks) as reported in Eq. (6). The parameters ($\varepsilon_i^0, \Delta\varepsilon_i^{close}$) and ($h_{22}^2, h_{44}^2, h_{66}^2$) are material coefficients which have to be identified. The effect tensors and the associated deactivation indexes for the other damage variables can be obtained through permutation of the indices.

$$\underline{\underline{H_2^m}} = \eta_2 \, \underline{\underline{H_2^{m+}}} \text{ with } \underline{\underline{H_2^{m+}}} = \begin{bmatrix} 0 & 0 & 0 & 0 & 0 & 0 \\ 0 & h_{22}^2 S_{22}^0 & 0 & 0 & 0 & 0 \\ 0 & 0 & 0 & 0 & 0 & 0 \\ 0 & 0 & 0 & h_{44}^2 S_{44}^0 & 0 & 0 \\ 0 & 0 & 0 & 0 & 0 & 0 \\ 0 & 0 & 0 & 0 & 0 & h_{66}^2 S_{66}^0 \end{bmatrix} \quad (5)$$

$$\text{with } \eta_2 = \begin{cases} 1 & \text{if} \quad \Delta\varepsilon_2^{close} \leqslant \varepsilon_2^d \\ \frac{1}{2}\left(1 - cos\left(\frac{\pi}{2} \frac{\varepsilon_2^d + \Delta\varepsilon_2^{close}}{\Delta\varepsilon_2^{close}} \right) \right) & \text{if} \quad \varepsilon_2^d \leqslant |\Delta\varepsilon_2^{close}| \quad \text{and} \quad \underline{\varepsilon}^d = \underline{\varepsilon} - \underline{\varepsilon}^0 \\ 0 & \text{if} \quad \varepsilon_2^d \leqslant -\Delta\varepsilon_2^{close} \end{cases} \quad (6)$$

Moreover, it is assumed that when a crack is closed, all the components of the elastic stiffness are restored, as reported in Eq. (5), even for the shear components. In order to ensure the continuity of the mechanical response for complex multiaxial loadings, a stored strain ($\underline{\varepsilon}^s$) has been introduced in the proposed modelling as

$$\dot{\underline{\varepsilon}}^s = -\underline{\underline{S}}^0 \sum_{i=1}^{2} \dot{\eta}_i \; d_i \; \underline{\underline{C}}^{eff} : \underline{\underline{\underline{\underline{H}}}}_i^{m+} : \underline{\underline{C}}^{eff} : (\underline{\varepsilon} - \underline{\varepsilon}^{ve} - \underline{\varepsilon}^0) \tag{7}$$

Special attention has been paid to the resolution of such a differential equation to obtain solutions which are insensitive to the size of the increment. This point is essential in order to perform impact simulations in a reasonable computational time when using a finite element code with an implicit solver.

3.4. Residual strains

Moreover, a residual strain ($\underline{\varepsilon}^r$) has been introduced into the present model and is defined as a function of the evolution of the damage variables as reported in Eq. (8). Its formulation is consistent with that proposed for the stored strain (see Eq. (7)).

$$\dot{\underline{\varepsilon}}^r = \underline{\underline{S}}^0 \sum_{i=1}^{2} \chi_i \; \dot{d}_i \; \underline{\underline{C}}^{eff} : \underline{\underline{\underline{\underline{H}}}}_i^{m} : \underline{\underline{C}}^{eff} : (\underline{\varepsilon} - \underline{\varepsilon}^{ve} - \underline{\varepsilon}^0) \tag{8}$$

The introduction of this residual strain is essential to predict the permanent indentation after impact, which is strongly connected to the in-plane mesoscopic damage, as proposed by [24,25]. The material coefficients χ_i can be directly identified on static tests. It can be noted that impact tests are thus not used for the identification of the residual strains and are considered in the following as validation tests.

3.5. Failure mechanisms

As for matrix damage, the failure patterns are clearly oriented by the microstructure of the material. The failure mechanisms in tension and in compression are very different and are thus considered separately. Two scalar failure variables are considered in the ODM-PMC model which are the yarn failure due to tensile loading in the weft and warp directions and noted, respectively, D_1^t and D_2^t. The two driving forces associated with failure of fibre yarns in tension ($y_1^{f^t}, y_2^{f^t}$) are defined in Eq. (9). After impact, only few fibre yarn failures are observed and predicted with the present approach.

$$y_j^{f^t} = \frac{1}{2} C_{jj}^0 \epsilon_{jj}^2 \quad \text{if } \epsilon_{jj} \geqslant 0 \text{with} j = \{1,2\} \tag{9}$$

In compression, the failure mechanism is very different and is due to fibre yarn kinking related to the specific architecture of the material. Two additional scalar failure variables are considered which are the yarn failure due to compressive loading in the weft and warp directions noted, respectively, D_1^c and D_2^c. The driving forces ($y_1^{f^c}, y_2^{f^c}$) are rather different from those in tension and are given in Eq. (10). It is an absolute necessity to take into account the influence of the hydrostatic pressure on the apparent onset of failure in compression in order to avoid predicting multiple yarn failures close to the impactor. Moreover, a strong coupling has been introduced between the compressive and shear stresses, these shear stresses promoting kinking of the fibre yarns as already proposed in [38–40].

$$\begin{cases} y_1^{f^c} = \sqrt{< \sigma_{11} - \sigma_{33} >_+^2 + a_1^t \tau_{13}^2} & \text{if } \epsilon_{11} < 0 \\ y_2^{f^c} = \sqrt{< \sigma_{22} - \sigma_{33} >_+^2 + a_2^t \tau_{23}^2} & \text{if } \epsilon_{22} < 0 \end{cases} \tag{10}$$

The progressive degradation laws associated with the yarn failures are reported in Eq. (11).

$$D_j^x = \left(\frac{< \sqrt{y_j^{D_x}} - \sqrt{y_j^{0\,D_x}} >_+}{\sqrt{y_j^{c\,D_x}}} \right)^{p_j^{D_x}} \quad \text{with} \quad x = (t,c) \quad \text{and} \quad j = \{1,2\} \tag{11}$$

where the parameter $y_j^{0\,D_x}$ corresponds to the onsets of yarn failure (equivalent to the failure of unnotched samples) in tension (noted with the index x = t) and in compression (noted with the index x = c) and ($y_j^{c\,D_x}, p_j^{D_x}$) are parameters related to the progressive degradation laws. The effect tensors $\underline{\underline{\underline{\underline{H}}}}_j^{D_x}$ associated with the failure of the fibre yarns, presented in Eq. (1), are similar to those defined in Eq. (5). The progressive degradation laws used for yarn failure are violent and usually catastrophic for the material and induce a softening behaviour.

4. Simulation of impact tests

4.1. Implementation in Abaqus/Standard

The ODM-PMC model has been implemented into the commercial finite element code Abaqus/Standard as a UMAT file. The choice of using a code with an implicit solver has been made in order to propose a two-step computing strategy which consists in predicting firstly the damage induced by an impact in a 3D woven composite and then to estimate the residual strengths of the specimen. The implicit FE code Abaqus/Standard and the material approach ODM-PMC are used for both the impact simulation and the estimation of the residual performances after impact. One of the objectives of this study is to transfer this methodology (model, identification procedure and numerical strategy) to design offices in aeronautical industries. Therefore, special attention has been paid to the computation of the consistent tangent matrix in order to improve the convergence of the simulation and to reduce the computational time. The macroscopic damage variables ($D_1^{t/c}, D_2^{t/c}, D_3$), describing the fibre yarn failures and the inter-yarn debondings, induce a violent and sudden decrease in the macroscopic rigidity, leading thus to a softening behaviour. Nevertheless, numerical problems are associated with this kind of modelling. For instance, the global response of the structure becomes dependent on the used mesh (type, size, and orientation of the elements of the mesh), inducing a loss of relevance in the performed finite element simulations. To avoid localisation problems, the introduction of a delay effect method [41,42] has been associated with the macroscopic damage variables. This regularisation method has been chosen mainly because it can be easily introduced into a commercial finite element code. For each failure mechanism, a characteristic time has to be introduced and identified. For impact loading, numerical parametric studies have shown that the through-the-thickness damage (D_3), representative of inter-yarn debondings, is the main dissipating energy mode. No (or only a few for the highest levels of energy) fibre yarn failure is observed. Therefore, in the present study, only the characteristic time associated with the inter-yarn debonding (D_3) has to be determined; this characteristic time is considered as a numerical parameter, and has thus been determined to avoid localisation problems.

4.2. Mesh and boundary conditions

The two configurations of impact tests have been considered. For configuration 1 with circular jaws, only the circular free zone of the plate is considered and according to symmetries, only one quarter of the system is represented. The impactor is modelled using an isotropic elastic behaviour law. The density of steel has

been attributed to the spherical part (bottom) of the impactor, while the density of the cylindrical part (above) has been adjusted in order to obtain the measured mass (14.8 kg) of the whole falling system. The ODM-PMC model has been used to model the behaviour of the composite plate. Frictionless contact is considered between the impactor and the plate. The boundary conditions of these finite element simulations are reported in Fig. 7a. Firstly, a spatial and temporal convergence study has been performed. The type (C3D8) and the size of the elements in the composite plate have been determined to obtain an interesting trade-off between the computational time and the description of driving force gradients. Moreover, the critical time step has been determined in order to capture the dynamical propagation which could induce damage for low-velocity/energy impacts.

For configuration 2, only one quarter of the system is represented. The impactor and one cylindrical support bar are modelled using an isotropic elastic behaviour law. Frictionless contact is considered between the impactor, one cylindrical bar and the plate. The boundary conditions of these finite element simulations are reported in Fig. 7b. A spatial and temporal convergence study for this configuration has also been performed to reduce the computational time.

4.3. Identification process

Some material parameters of the ODM-PMC model have already been identified through static tests (tension, compression or creep...) on unnotched specimens [30,31]. The onsets of damage and failure in the warp and weft directions have been determined through the analysis of off-axis tensile tests (at 0°, 45°, 90°). Moreover, the parameters related to the evolution law of the in-plane mesoscopic damage variables (d_1, d_2) and their associated effects have also been estimated. Finally, thanks to incremental tensile tests, the parameters χ_i, related to the residual strain, have also been determined. Fig. 8 presents the comparison between the predictions and the experimental data from some off-axis incremental tensile tests on unnotched specimens at 0°and 22, 5°.

Nevertheless, the through-the-thickness properties are still difficult to identify on simple tests but their identification can be performed only on structures. Classical InterLaminar Shear Stress tests [43] have been performed on short beams to estimate the out-of-plane shear modulus and the onset of damage. Additional four-point bending tests on L-angle specimens [44,45] have been performed to estimate the out-of-plane modulus and the onset of debonding for out-of-plane tensile loading. Nevertheless, for these tests, since inter-yarn debondings appear, the decrease in the rigidity is violent and it is not suitable to identify the parameters of the evolution law on these tests. This point is still a challenge and some future works will be performed on that topic.

Preliminary finite element simulations performed using an orthotropic elastic behaviour for the composite plate have demonstrated the necessity to take into account the different damage mechanisms in the simulations, as reported in Fig. 9. Then, parametric studies using the ODM-PMC model have demonstrated that the through-the-thickness damage (D_3) is the main dissipating energy mode for impact loading. Therefore, in this study, the through-the-thickness damage properties (evolution law parameters and the associated characteristic time) of the ODM-PMC model have been identified on the 150 J impact test in such a way that the peak force, the dissipated energy and the spread of the damaged zones are described accurately by the model as compared to the available experimental data reported in Fig. 9.

Then, to validate the model and the associated identification process, different simulations with different levels of impact energy and different boundary conditions have been performed and compared with impact tests.

4.4. Comparisons with experimental data

Firstly, the global response of the tested composite plates are compared with the predictions of the model for a large range of energy levels (from 40 J to 210 J) and different impact testing conditions. Concerning the experimental force/time curves, it can be noted that two different kinds of periodic oscillations are recorded: (i) a first one which corresponds to vibrations of the composite plate (with a short period of around 0.1 ms) and (ii) a second kind associated with vibrations of the whole experimental device (with a large period around 0.8 ms). Impact tests on aluminium plates have been performed in order to confirm the previous conclusions. It can be noted that the load/time curves do not present severe discontinuities as observed for laminated composite materials [11] because only diffuse damage mechanisms are observed within 3D woven composite materials. The model is able to describe correctly the impact behaviour for different energy levels (from 40 J to 210 J), as reported in Fig. 10, even impacts on simply supported plates. However, the large period oscillations are not captured by the proposed modelling because the experimental setup has not been taken into account in finite element simulations. The

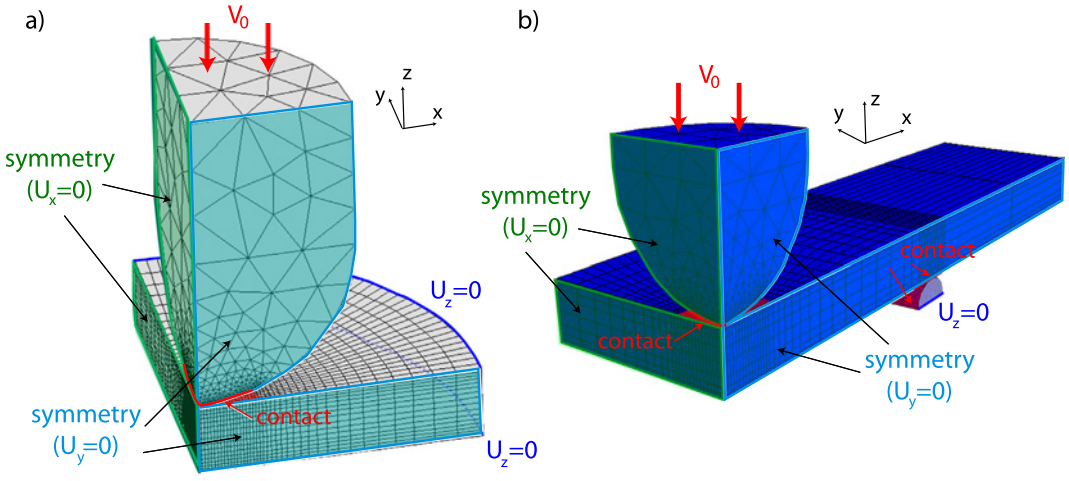

Fig. 7. Boundary conditions used for the two configurations of impact tests: (a) configuration 1 (with circular jaws) and (b) configuration 2 (simply supported) where the x-direction is aligned with the warp direction.

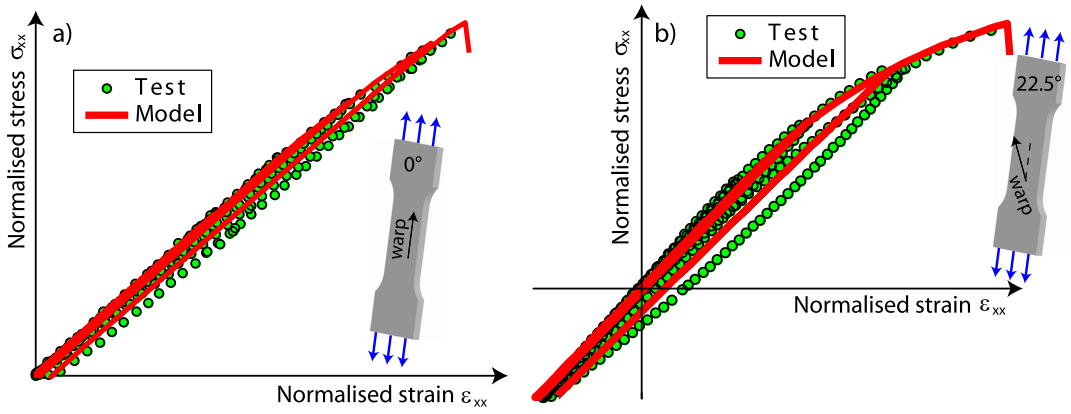

Fig. 8. Predicted and experimental stress/strain curves of a 3D woven composite subjected to off-axis incremental tensile loading at (a) 0°and (b) 22.5°.

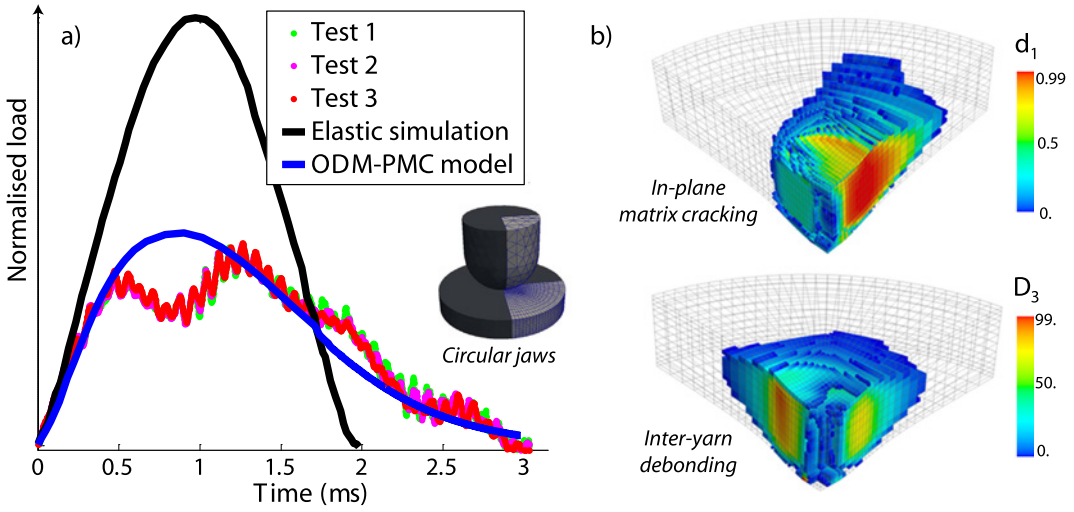

Fig. 9. Identification of through-the-thickness damage parameters through the comparisons with (a) the impact load versus time history curves and (b) the damaged area for a 150 J impacted 3D woven plate for configuration 1.

predicted peak loads are in very good agreement with those measured for all the considered configurations and all the tested energy levels. Nevertheless, the duration of contact is slightly overestimated for the different energy levels, but remains acceptable.

The prediction of shear matrix cracks and inter-yarn debondings distribution is in good agreement with the experimental observations reported in Fig. 11, and presents a typical pattern which is strongly correlated to the out-of-plane shear stress gradient through the thickness. However, the debondings extent is slightly overestimated with the model but their magnitudes remain consistent with experimental observations. The impact axis is preserved from matrix damage in both simulation and test results due to the influence of the hydrostatic pressure. Matrix cracking on the back face, due to local tensile loading, is also very well captured by the proposed modelling. Concerning the yarn failures, the introduction of the hydrostatic pressure enables to limit the occurence of failures in compression under the impactor as observed experimentally. Moreover, on the back face of the plate, the few yarn failures, created under local tension, are described with the model according to experimental observations. It is also worth mentioning that computational times obtained with the finite element code Abaqus/Standard for the different energy levels remain acceptable even for a design office (from 2 h for impact simulation at 60 J to 5 h for impact simulation at 210 J).

The residual dent (indentation depth) is a characteristic indicator of impact and thus of induced damage within the composite material. The estimation of its depth enables to establish relationships between the dent and the damaged area as usually performed for laminates (mostly experimentally). In this study, the dent is accurately predicted with the ODM-PMC model thanks to the introduction of the residual strain, identified through the analysis of static tests. The depth of the indentation has been numerically determined as the maximal out-of-plane displacement when the impactor is no longer in contact with the plate. The estimated dent can be considered as a permanent dent (relaxation due to the viscosity of the matrix remains low as observed experimentally and numerically). An excellent agreement between the experimental data in the considered energy range and the predictions is observed in Fig. 12.

All these comparisons between the impact predictions and the experimental results have demonstrated the ODM-PMC model's ability to estimate both global (maximal peak force) and local (distribution and size of the damaged area) quantities correctly whereas the computational times remain rather low (only a few hours). The efficiency of the model has also been demonstrated for the prediction of the permanent dent, so that relationships between impact parameters (incident energy, permanent dent, damaged area), usually determined through experiments, can now be numerically estimated for 3D woven composites.

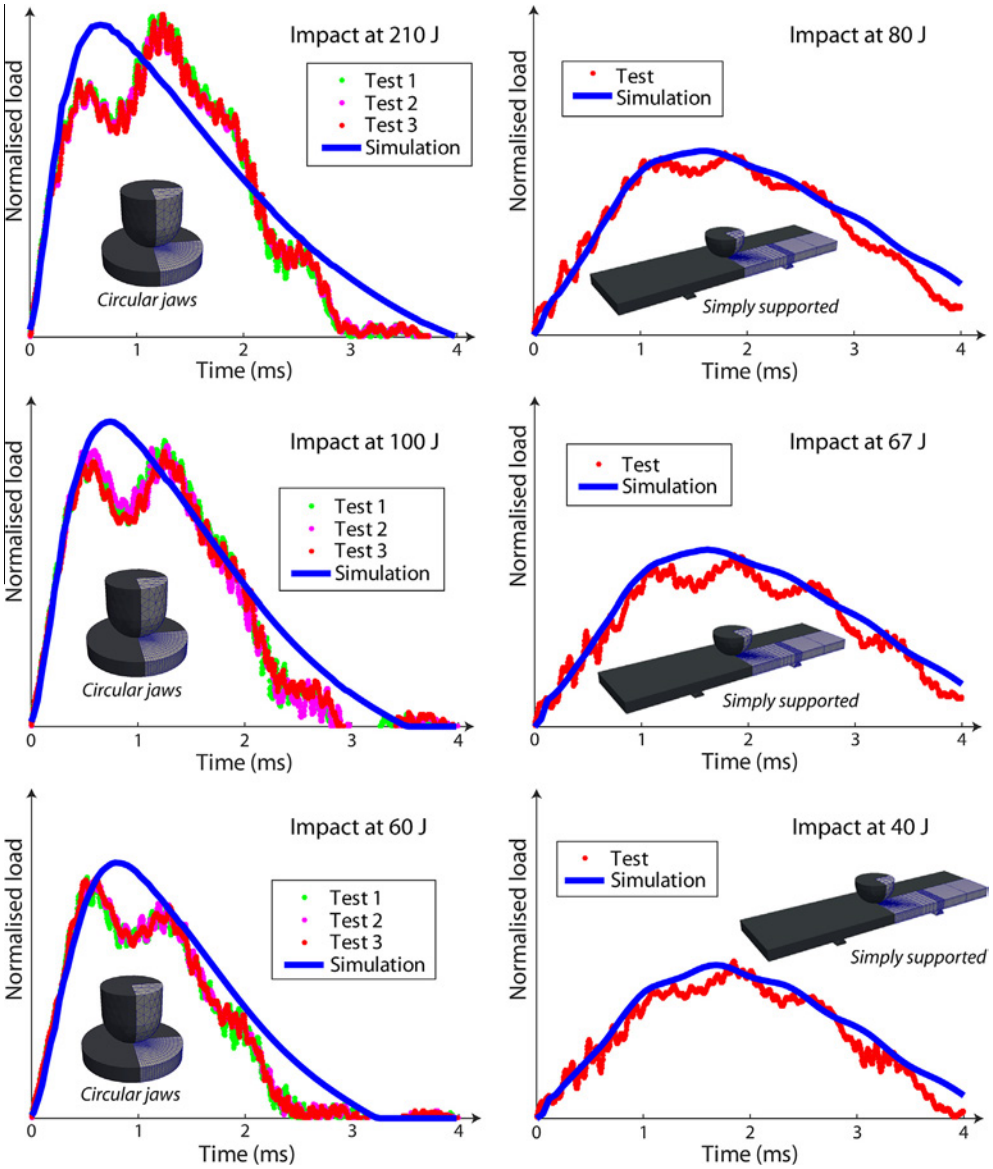

Fig. 10. Comparison between the predicted and measured force versus time history at different energy levels for the two configurations of impact tests.

In order to demonstrate that these conclusions can be generalised to other 3D architectures, a complementary experimental study has also been performed on another 3D highly unbalanced woven composite material provided by Safran group. The total thickness and the size of the RVE are rather similar to those of the previous material. Some additional impact tests have been performed at Onera, using the test configuration 1 (with circular jaws), at 3 different energy levels [37], inferior to 160 J. Firstly, the shape of the projected damaged area is more elliptical than previously because a highly unbalanced woven material is considered here. Moreover, the measured projected damage areas and the residual depths are different from those measured previously on the moderately unbalanced material, thereby confirming that the choice of the architecture plays a major role in the values of these quantities. Nevertheless, the damage patterns remain very similar (inter-yarn debondings and matrix cracking) and only diffuse damage mechanisms are observed (no large delamination crack). Using a continuum damage approach, as the ODM-PMC approach, is again relevant for this alternative material. The macroscopic ODM-PMC approach has been identified for this highly unbalanced 3D woven composite material, as detailed in Section 4.3, because the mesoscopic architecture is different. Then, the predicted quantities (projected damage areas and permanent dents) have been compared quite successfully with the few available tests. The present approach can thus be applied to 3D woven composite materials different from those presented in this paper, as long as only diffuse damage mechanisms are observed within the impacted specimens.

5. Conclusions

Low-velocity/energy impacts on 3D woven composites have been studied experimentally and numerically in order to improve the understanding of damage mechanisms in these recent materials. Impact tests have been performed at different energy levels and using two different experimental setups in order to obtain a large experimental data base and thus to validate the model. Different measurement techniques (C-Scan, microscopic observations, X-ray tomography ...) have been used to demonstrate that only diffuse damage is generated in 3D woven composites after impacts. That point constitutes a major difference compared with lami-

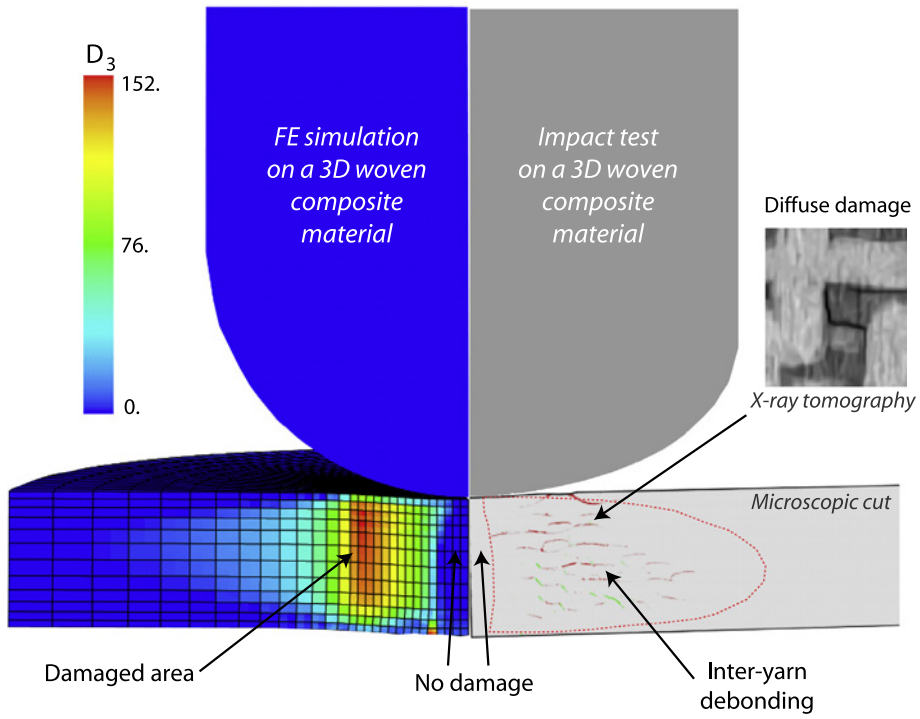

Fig. 11. Comparison between the predicted damaged area and experimental observations (microscopic cut and X-ray tomography) in an impacted 3D woven plate for configuration 1.

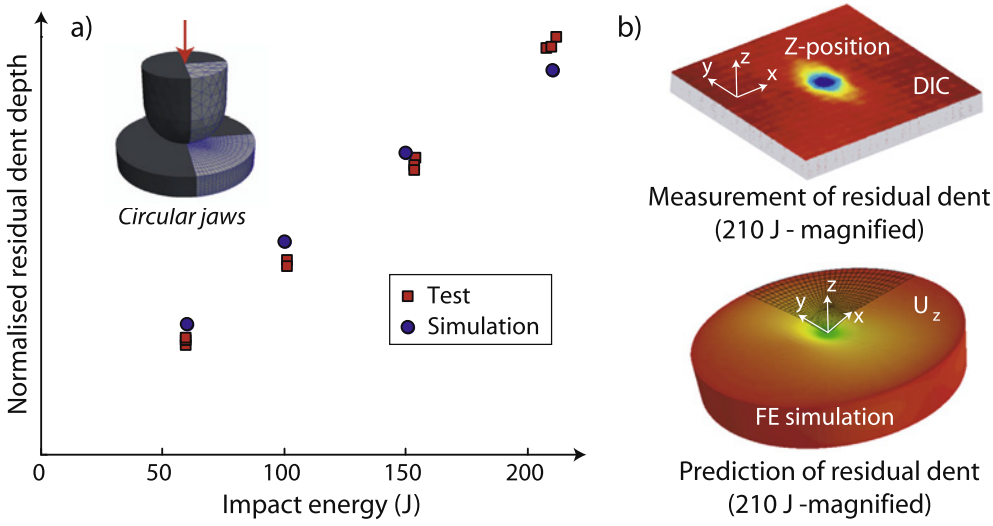

Fig. 12. (a) Comparison between predicted and measured indentation depths by stereo-digital images correlation for different levels of impact energy for configuration 1, (b) predicted and measured indentation for a 210 J impacted 3D woven plate.

nates, in which large delamination cracks are observed after impact. These damage mechanisms are mainly inter-yarn debondings and a few in-plane matrix cracks.

In the present article, the predictive capabilities of the Onera Damage Model for Polymer Matrix Composites, already validated for in-plane static or fatigue loadings, are evaluated for impact cases. Finite element simulations have allowed explaining the origin of the observed shape of the damage pattern, which essentially results from the inter-laminar shear stresses through the thickness and also from local tensile loading in the back face of the plate. This model has been implemented in the commercial finite element code Abaqus/Standard to simulate the different impact tests with reasonable computational times (a few hours). It seems that impact damage mechanisms are described accurately by the model. Moreover, the predictions of impact damage and impact responses obtained with this approach are in good agreement with the available experiments.

The next step consists in predicting the static residual strengths after impact of 3D woven composites. A two-step simulation method is proposed and consists in predicting first the damage induced by an impact in a 3D woven composite material and then in estimating the residual strengths of the specimen. The same constitutive equations (ODM-PMC) and the same implicit finite element code Abaqus/Standard are used both for the estimation

of damage during impact and for the simulation of the static loadings after impact to estimate the residual properties of the material.

Acknowledgements

The collaboration with Snecma and Messier-Bugatti-Dowty is gratefully acknowledged. This work was supported under the PRC Composites, French research project funded by DGAC, involving SAFRAN Group, ONERA and CNRS. The authors would like to express their sincere gratitude to Dr. R. Valle, for valuable and helpful discussions.

References

[1] Abrate S. Impact on composite structures. Cambridge University Press; 1998, ISBN 9780511574504. Cambridge Books Online.
[2] Cantwell WJ, Morton J. The impact resistance of composite materials – a review. Composites 1991;22:347–62.
[3] Davies GO, Olsson R. Impact on composite structures. Aeronaut. J. 2004;108:541–63.
[4] Bibo GA, Hogg PJ. The role of reinforcement architecture on impact damage mechanisms and post-impact compression behaviour. J. Mater. Sci. 1996;31 (5):1115–37.
[5] de Freitas M, Silva A, Reis L. Numerical evaluation of failure mechanisms on composite specimens subjected to impact loading. Compos Part B: Eng 2000;31(3):199–207.
[6] Richardson M, Wisheart M. Review of low-velocity impact properties of composite materials. Compos Part A: Appl Sci Manuf 1996;27(12):1123–31.
[7] de Freitas M, Reis L. Failure mechanisms on composite specimens subjected to compression after impact. Compos Struct 1998;42(4):365–73.
[8] Lopes CS, Camanho PP, Gurdal Z, Maimi P, Gonzalez EV. Low-velocity impact damage on dispersed stacking sequence laminates. Part II: numerical simulations. Compos Sci Technol 2009;69(7–8):937–47.
[9] Petit S, Bouvet C, Bergerot A, Barrau JJ. Impact and compression after impact experimental study of a composite laminate with a cork thermal shield. Compos Sci Technol 2007;67(15–16):3286–99.
[10] Bull DJ, Spearing SM, Sinclair I. Observations of damage development from compression-after-impact experiments using ex situ micro-focus computed tomography. Compos Sci Technol 2014;97:106–14.
[11] Hongkarnjanakul N, Bouvet C, Rivallant S. Validation of low velocity impact modelling on different stacking sequences of CFRP laminates and influence of fibre failure. Compos Struct 2013;106:549–59.
[12] Pernas-Sãnchez J, Artero-Guerrero JA, Viñuela J, Varas D. Numerical analysis of high velocity impacts on unidirectional laminates. Compos Struct 2014;107:629–34.
[13] Artero-Guerrero JA, Pernas-Sãnchez J, Lõpez-Puente J, Varas D. On the influence of filling level in CFRP aircraft fuel tank subjected to high velocity impacts. Compos Struct 2014;107:570–7.
[14] Gonzalez EV, Maimi P, Camanho PP, Turon A, Mayugo JA. Simulation of drop-weight impact and compression after impact tests on composite laminates. Compos Struct 2012;94(11):3364–78.
[15] Rivallant S, Bouvet C, Hongkarnjanakul N. Failure analysis of CFRP laminates subjected to compression after impact: FE simulation using discrete interface elements. Compos Part A: Appl Sci Manuf 2013;55:83–93.
[16] Chiu CH, Lai MH, Wu CM. Compression failure mechanisms of 3-D angle interlock woven composites subjected to low-energy impact. Polym Polym Comp 2004;12(4):309–20.
[17] Chen F, Hodgkinson JM. Impact behaviour of composites with different fibre architecture. Proc Inst Mech Eng, Part G: J Aerosp Eng 2009;223(7):1009–17.
[18] Heimbs S, Van Den Broucke B, Duplessis Kergomard Y, Dau F, Malherbe B. Rubber impact on 3D textile composites. Appl Comp Mater 2011;19 (3):275–95.
[19] Henry J, Aboura Z, Khellil K, Otin S. Suivi de l'endommagement en fatigue d'un composite á renfort interlock carbone/epoxy par émission acoustique. JNC17 – 17iéme Journées Nationales des Composites. Poitiers, France: AMAC; 2011.
[20] ASTM. Standard test method for measuring the damage resistance of a fiber-reinforced polymer matrix composite to a drop-weight impact event. Standard D7136/D7136M-07; 2007.
[21] Carrere N, Laurin F, Maire J-F. Micromechanical-based hybrid mesoscopic 3D approach for non-linear progressive failure analysis of composite structures. J Compos Mater 2012;46(19–20):2389–415.
[22] McCombe G, Rouse J, Trask R, Withers P, Bond I. X-ray damage characterisation in self-healing fibre reinforced polymers. Compos Part A: Appl Sci Manuf 2012;43(4):613–20.
[23] Seltzer R, Gonzalez C, Munoz R, LLorca J, Blanco-Varela T. X-ray microtomography analysis of the damage micromechanisms in 3D woven composites under low-velocity impact. Compos Part A: Appl Sci Manuf 2013;45:49–60.
[24] Bouvet C, Rivallant S, Barrau JJ. Low velocity impact modeling in composite laminates capturing permanent indentation. Compos Sci Technol 2012;72 (16):1977–88.
[25] Hongkarnjanakul N, Rivallant S, Bouvet C, Miranda A. Permanent indentation characterization for low-velocity impact modelling using three-point bending test. J Compos Mater 2014;48(20):2441–54.
[26] Maire J-F, Chaboche J-L. A new formulation of continuum damage mechanics (CDM) for composite materials. Aerosp Sci Technol 1997;1(4):247–57.
[27] Schneider J. Mécanismes d'endommagement dans les composites multicouches à renforts interlock. Technological University of Compiègne; 2011. Doctorate thesis.
[28] Henry J. Etude et analyse des mécanismes d'endommagements en fatigue des composites à renforts tissés interlocks. Technological University of Compiègne; 2013. Doctorate thesis.
[29] Hurmane A. Analyse par un dialogue essais/calculs de la tenue en compression de structures composites tissées 3D. Technological University of Compiègne, 2015. Doctorate thesis.
[30] Marcin L. Modélisation du comportement, de l'endommagement et de la rupture des matériaux composites à renforts tissés pour le dimensionnement robuste de structures. University of Bordeaux I; 2010. Doctorate thesis.
[31] Rakotoarisoa C. Prévision de la durée de vie en fatigue des composites à matrice organique tissés interlock. Technological University of Compiègne; 2013. Doctorate thesis.
[32] Laurin F, Carrere N, Maire J-F. A multiscale progressive failure approach for composite laminates based on thermodynamical viscoelastic and damage. Compos Part A: Appl Sci Manuf 2007;38(1):198–209.
[33] Laurin F, Carrere N, Huchette C, Maire J-F. A multiscale hybrid approach for damage and final failure predictions of composite structures. J Compos Mater 2013;47(20–21):2713–47.
[34] Ju JW. On energy-based coupled elastoplastic damage theories: constitutive modeling and computational aspects. Int J Solids Struct 1989;25:803–33.
[35] Maire J-F, Pacou D. Essais de traction-compression-torsion sur tubes composites céramique-céramique. JNC10 – 10ième Journées Nationales des Composites, vol. 3. Paris, France: AMAC; 1996. p. 1226–34.
[36] Puck A, Schurmann H. Failure analysis of FRP laminates by means of physically based phenomenological models. Compos Sci Technol 2002;62(12):1633–62.
[37] Elias A. Nocivité des défauts induits par impact pour les structures composites tissées 3D à matrice organique. Ecole Centrale Nantes; 2015. Doctorate thesis.
[38] Jelf PM, Fleck NA. Compression failure mechanisms in unidirectional composites. J Compos Mater 1992;26(18):2706–26.
[39] Pimenta S, Gutkin R, Pinho ST, Robinson P. A micromechanical model for kink-band formation: Part I: experimental study and numerical modelling. Compos Sci Technol 2009;69(7–8):948–55.
[40] Gutkin R. Understanding and modelling failure of laminated composites. Imperial College of London; 2010. Ph. D. thesis.
[41] Duvaut G, Lions JL. Inequalities in mechanics and physics. Berlin Heidelberg: Springer-Verlag; 1976.
[42] Marcin L, Maire JF, Carrere N, Martin E. Development of a macroscopic damage model for woven ceramic matrix composites. Int J Damage Mech 2011;20 (6):939–57.
[43] ASTM. Standard test method for short-beam strength polymer matrix composite materials and their laminates. Standard D2344/D2344M-06a; 2006.
[44] ASTM. Standard test method for measuring the curved beam strength of fiber reinforced polymer matrix composite. Standard D6415/D6415M-06a; 2006.
[45] Charrier JS, Laurin F, Carrere N, Mahdi S. Determination of the out-of-plane tensile strength using four-point bending tests on laminated L-angle specimens with different stacking sequences and total thicknesses. Compos Part A: Appl Sci Manuf 2016;81:243–53.